

# Single droplet combustion of decane in microgravity: experiments and numerical modeling

D L Dietrich†, P M Strukt†, M Ikegami‡ and G Xu‡

† NASA John H. Glenn Research Center, Cleveland, Ohio 44135 USA

‡ National Institute for Advanced Industrial Science and Technology, Hokkaido, JAPAN

**Abstract.** This paper presents experimental data on single droplet combustion of decane in microgravity and compares the results to a numerical model. The primary independent experiment variables are the ambient pressure and oxygen mole fraction, pressure, droplet size (over a relatively small range) and ignition energy. The droplet history ( $D^2$  history) is non-linear with the burning rate constant increasing throughout the test. The average burning rate constant, consistent with classical theory, increased with increasing ambient oxygen mole fraction and was nearly independent of pressure, initial droplet size and ignition energy. The flame typically increased in size initially, and then decreased in size, in response to the shrinking droplet. The flame standoff increased linearly for the majority of the droplet lifetime. The flame surrounding the droplet extinguished at a finite droplet size at lower ambient pressures and an oxygen mole fraction of 0.15. The extinction droplet size increased with decreasing pressure.

The model is transient and assumes spherical symmetry, constant thermo-physical properties (specific heat, thermal conductivity and species Lewis number) and single step chemistry. The model includes gas-phase radiative loss and a spherically symmetric, transient liquid phase. The model accurately predicts the droplet and flame histories of the experiments. Good agreement requires that the ignition in the experiment be reasonably approximated in the model and that the model accurately predict the pre-ignition vaporization of the droplet. The model does not accurately predict the dependence of extinction droplet diameter on pressure, a result of the simplified chemistry in the model. The transient flame behavior suggests the potential importance of fuel vapor accumulation. The model results, however, show that the fractional mass consumption rate of fuel <sup>in</sup> the flame is close to 1.0 for all but the lowest ambient oxygen mole fractions.

relative to fuel vaporized

Submitted to: *Combust. Theory Modelling*

This report is a preprint of an article submitted to a journal for publication. Because of changes that may be made before formal publication, this preprint is made available with the understanding that it will not be cited or reproduced without the permission of the author.

## 1. Introduction

Theories and experiments involving single droplet combustion date back to 1953 [1], with the first microgravity work appearing in 1956 [2]. The problem of a spherical droplet burning in an infinite, quiescent, microgravity environment is a classic problem in combustion research with the simplified solution appearing in nearly every textbook on combustion (e.g. [3]). This simplified solution predicts that the decrease of the droplet diameter squared with time is a constant (d-squared law) ( $\bar{k}$ ). The solution also predicts that the ratio of the flame diameter ( $D_f$ ) to the droplet diameter ( $D$ ) is constant and independent of time or droplet diameter.

Because of the ideal geometry and one dimensional nature of the problem, spherically symmetric droplet combustion has been extensively studied. The microgravity environment offered by ground-based facilities such as drop towers and space-based platforms, is ideal for studying the problem experimentally. Indeed as a recent review by Choi and Dryer[4] shows, significant advances in droplet combustion have been made by studying the problem experimentally in microgravity and comparing the results to one dimensional (spatially) theoretical and numerical treatments of the problem.

The classical analysis makes several simplifying assumptions, including a quasi-steady gas-phase, constant thermo-physical properties, unity Lewis number, and infinitely fast chemical kinetics. These assumptions provide valuable qualitative insight into the physics of droplet combustion but make quantitative agreement with experiments difficult. The classical analysis can produce reasonable estimates of  $\bar{k}$  (with properly chosen thermo-physical properties). Estimates of  $D_f$ , however, often differ from experimental values by a factor of five or more. Further, the classical analysis cannot predict flame extinction. Current theoretical (e.g. [5]) and numerical (e.g. [6]) models relax many of these assumptions and show better agreement with experimental data. To fully exercise the capabilities of these models and improve them, researchers require access to single droplet combustion data over a range of fuels and ambient conditions.

In this article, we present the results of single droplet combustion experiments and compare the results to a numerical model. The fuel for all of the experiments was decane. The independent experiment variables were the ambient pressure, oxygen mole fraction, initial droplet size, and ignition energy. The model is transient and includes single-step, finite-rate chemistry and flame zone radiative loss.

## 2. Experiments

### 2.1. Experimental Apparatus

Because complete details of the experimental hardware are available elsewhere[7] only a brief description is provided here. A 125 or 230 $\mu\text{m}$  fiber with a small bead ( $\approx 2x$  the fiber diameter) supported droplets with an initial diameter between 0.9 $\text{mm}$  and 1.8 $\text{mm}$ . A stepper motor driven syringe dispensed the fuel droplets onto the ends of the fibers.

in normal gravity just before the drop. A small coiled hot-wire, withdrawn immediately after ignition, ignited the droplets in microgravity. The ignition duration was typically on the order of 1 s. During this time the battery delivered approximately 40J of energy to the hot wire. A simplified thermal analysis of the hot-wire shows that approximately 10 percent of this (i.e. 4J) actually heated the gas-phase surrounding the droplet during the 1s ignition time. The rest of the energy heated the wire or radiated to the chamber walls. For reference, the total energy released in burning a 1.5mm decane droplet is approximately 60J.

The atmospheres were blends of air† and nitrogen, mixed by partial pressures. We estimate the oxygen mole fraction ( $X_{O_2}$ ) to be  $\pm 0.002$  of the stated value, and the pressure ( $P$ ) to be accurate to 1 percent of the indicated value. The uncertainty in the atmosphere comes from uncertainty in the chamber pressure, small leaks in the combustion chamber, and errors that result from the finite volume of the gas supply tubing.

The data for experiments were video recordings from two orthogonally located, black and white CCD video cameras. The first camera provided a magnified backlit view of the droplet to obtain the droplet regression history. The second view was of the flame and had a small 15  $\mu m$  diameter SiC fiber in the field-of-view (passing through the center of the droplet). Radiant emission from this small fiber helped determine the presence (or lack thereof) of the flame in ambient conditions in which the CCD camera could not image the dim flame.

A microcomputer equipped with a black and white frame-grabbing board analyzed the video data from the experiments. The droplet diameter in this article is the size that results from equating the measured volume or projected area of the droplet to that of the equivalent sphere or circle, respectively[8]. In reporting the burning rate of the fuel droplet, we present both an average ( $\bar{k}$ ) and an instantaneous ( $k$ ) burning rate constant. The  $\bar{k}$  comes from a linear fit of the data between  $\tilde{t} = 0.1\tilde{t}_b$  and  $0.9\tilde{t}_b$ , where  $\tilde{t}_b$  is the total burn time (igniter withdraw to extinction or burnout) and  $\tilde{t}$  is the time ( $t$ ) normalized by the initial droplet diameter squared ( $D_0^2$ ). The  $k$  comes from a modified cubic spline fit routine applied to the experimental data. In this method, the droplet history ( $(D/D_0)^2$  as a function of  $\tilde{t}$ ) is divided into equally-sized discrete intervals ( $\Delta\tilde{t}$ ). A best-fit third order polynomial is found for each interval, subject to the constraint that at each node point there is continuity in  $(D/D_0)^2$ , its first ( $k$ ) and second ( $\dot{k}$ ) derivatives. The  $k$  at any time is then the derivative of the best-fit polynomial for that particular interval. We found that this provides an excellent fit to the experimental data.

† The air was a precision gas blend of oxygen (0.21 mole fraction) and nitrogen mixed gravimetrically by the manufacturer.

## 2.2. Experimental Results

Figure 1 shows the burning history for a single 1.7mm decane droplet in a  $P = 190\text{mmHg}$ ,  $X_{O_2} = 0.17$  ambient. This test exhibits many features typical to all of the tests and is also one of the base cases used in the refinement of the numerical model (described later). The droplet burning history is non-linear. There is a small decrease in  $k$  initially which is probably due to the presence of the igniter. The igniter is a heat source which provides extra energy for vaporization and it is reasonable to expect a small transient associated with the withdraw. After this short decrease,  $k$  increases slowly from 0.5 to  $0.6\text{mm}^2/\text{s}$  until the middle of the test. This increase could be the result of a number of transient phenomena in droplet combustion, such as transient heating of the liquid phase[9] and/or fuel vapor accumulation[24]. The magnitude and time-scale of the increase are consistent with both phenomena. The  $k$  then increases slightly until the end of the burn, where it increases more quickly until extinction or burnout.

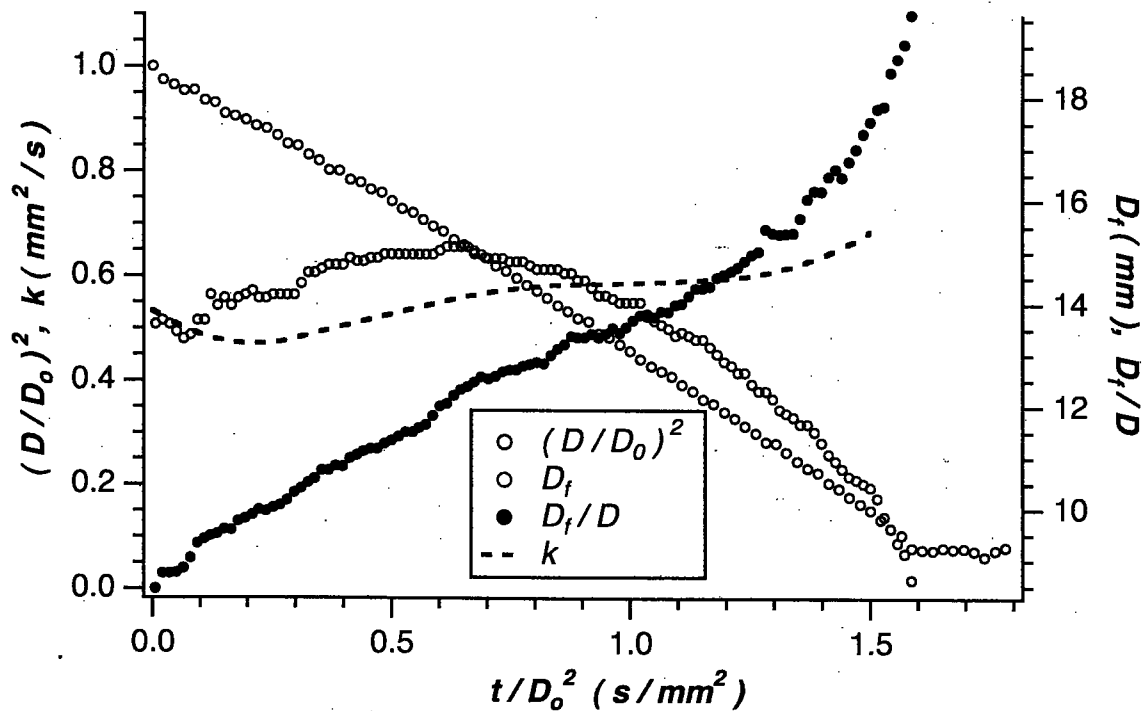


Figure 1. Combustion history of a decane droplet initially 1.7 mm in diameter burning in a  $X_{O_2} = 0.17$ , 190mmHg ambient. The graph shows a sparse subset of the experimental data for clarity.

The flame behavior in Figure 1 is characteristic of that in most of the nitrogen-diluted tests. The flame diameter ( $D_f$ ) initially increases in size, plateaus for a significant period of time in the middle of the test, and then decreases until the end of the test. After reaching the maximum value, the flame responds to the shrinking

droplet, although the droplet size decreases 25 percent before the flame responds.

Finally, Figure 1 shows that the flame standoff ratio ( $D_f/D$ ) continuously increases from ignition until extinction. This increase was characteristic of all the nitrogen-diluted tests. The rate of increase is nearly constant (linear slope) until late in the burn. Close to extinction or burnout, the standoff ratio increases faster.

Figure 2 shows the effect of ambient oxygen mole fraction at  $P = 190 \text{ mmHg}$  and  $D_0 = 1.6 \text{ mm}$  ( $\pm 0.1 \text{ mm}$ ) for each test. Both the droplet and flame behavior are qualitatively consistent with the classical analysis of single droplet combustion. The values of  $\bar{k}$  for the  $X_{O_2} = 0.15, 0.17$  and  $0.19$  tests are  $0.52, 0.57$ , and  $0.65 \text{ mm}^2/\text{s}$ , respectively. The relative dependence on ambient oxygen mole fraction is very close to that predicted by classical droplet combustion theory[3]. The flame size increases with decreasing ambient oxygen mole fraction. All three tests show the same qualitative trend of the flame size increases, reaching a maximum, and decreasing until burnout. The flame standoff also increases with decreasing ambient oxygen mole fraction, although the differences are small between the two smallest ambient oxygen mole fraction ambients. The flame standoff increases almost linearly with time for all of the tests.

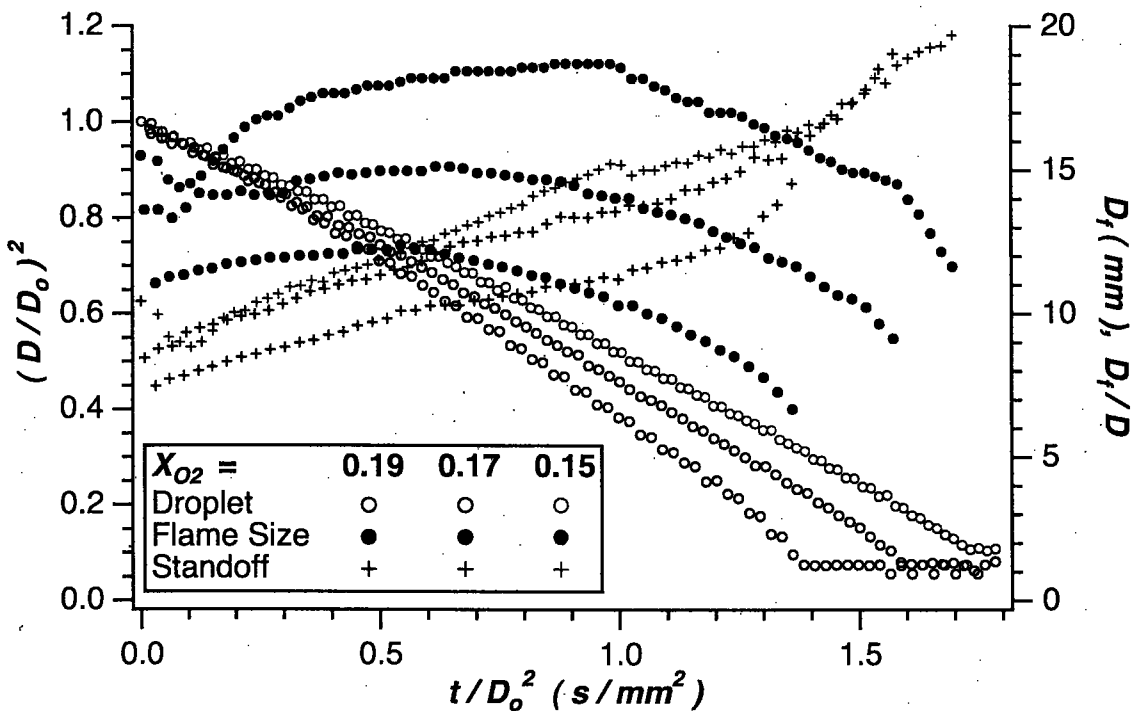


Figure 2. Combustion histories for three experiments ( $D_0 \approx 1.6 \text{ mm}$ ) burning in  $190 \text{ mmHg}$ , and  $X_{O_2} = 0.15, 0.17$  and  $0.19$  ambients. The graph shows a sparse subset of the experimental data for clarity.

Figure 3 shows the influence of ambient pressure on the burning history of four droplets ( $D_0 \approx 1.7 \text{ mm} \pm 0.1 \text{ mm}$ ) burning in ambients with  $X_{O_2} = 0.15$ . The droplet

regression histories for these tests are nearly identical, with the variation in  $\bar{k}$  (and  $k$ ) less than 10 percent of the average value of  $0.52\text{mm}^2/\text{s}$ . The  $k$  starts at approximately  $0.46\text{mm}^2/\text{s}$  and increases throughout the droplet lifetime to approximately  $0.65\text{mm}^2/\text{s}$  at the end of the test. At pressures below  $190\text{mmHg}$ , the flame extinguishes at a finite droplet size. The extinction droplet diameter,  $D_{ext}$ , increases with decreasing pressure. At  $90\text{mmHg}$ , the droplet burns for only a short time before flame extinction.

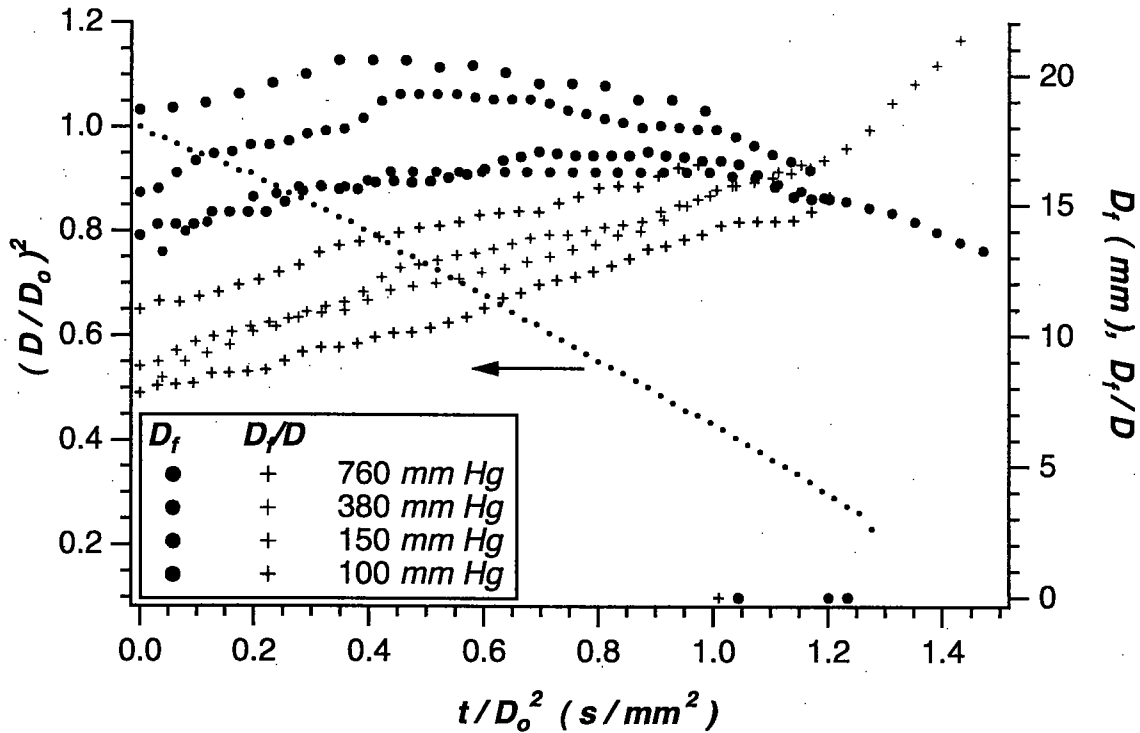


Figure 3. Combustion histories for four experiments ( $D_0 \approx 1.7\text{mm}$ ) burning in  $X_{O_2} = 0.15$  and  $P = 760, 380, 150$  and  $100\text{mmHg}$  ambients. The droplet histories were nearly identical for all of the tests, so only one is displayed. The graph shows a sparse subset of the experimental data for clarity.

While the droplet behavior was nearly independent of pressure, Figure 3 shows that at pressures below  $380\text{mmHg}$ , the flame size (at a given  $\bar{t}$ ) increases with decreasing pressure, as does  $D_f/D$ . These increases are consistent with the effects of finite rate chemical kinetics that slow the chemical reaction rate down (increasing characteristic chemical time) with decreasing pressure.

Figure 4 shows the effect of initial droplet size for droplets burning in a  $100\text{mmHg}$ ,  $0.15$  oxygen mole fraction ambient. The flames surrounding droplets burning in this ambient pressure and oxygen mole fraction extinguish at a finite droplet size. The results show that  $\bar{k}$  did increase with increasing droplet size. The change, however, was less than 10 percent over the range of droplet sizes. As one expects, the flame size increases with increasing droplet size. The flame standoff dependence on droplet size is not as intuitive. The two larger droplets show a consistent, nearly linear increase

over the entire droplet burning history. The flame standoff for the smallest droplet, however, increases at a slower rate than the two larger droplets, and then reaches an almost constant value for the last one third of the burn time. Finally, Fig. 4 shows that  $D_{ext}$  (i.e. extinction droplet diameter) increases with increasing  $D_0$ .

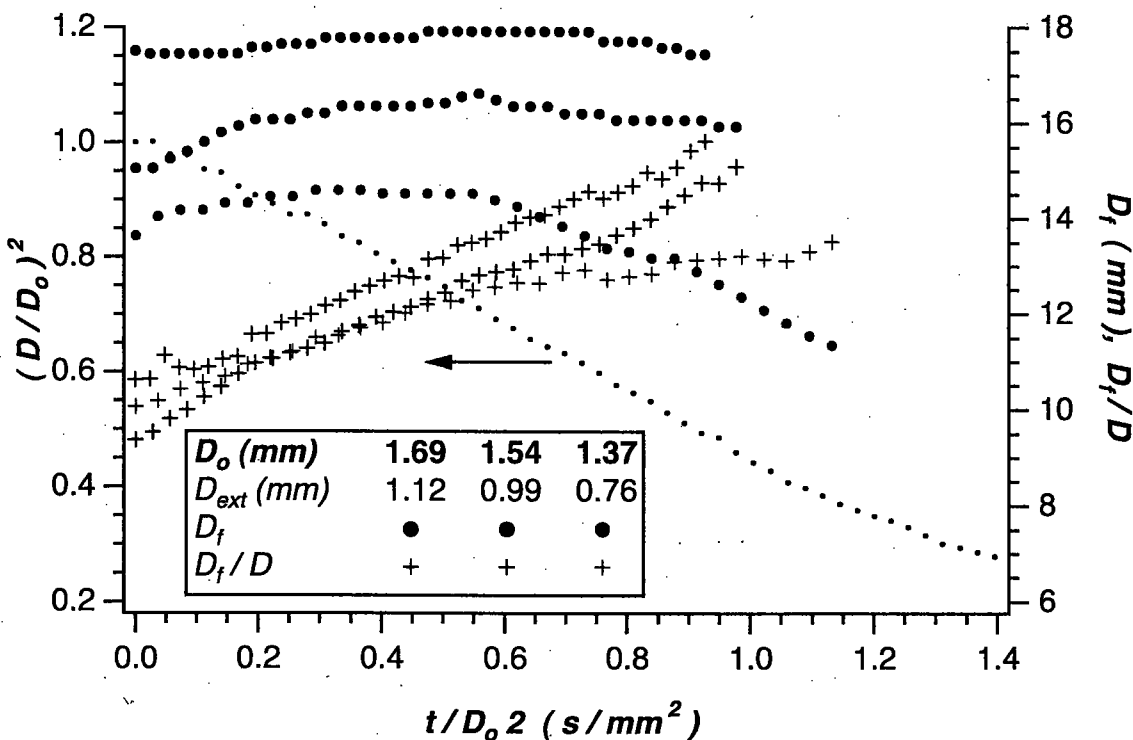


Figure 4. Combustion histories for three experiments with different initial droplet diameters burning in  $X_{O_2} = 0.15$  and  $P = 100\text{mm.Hg}$  ambients. The droplet regression histories are similar for all of the tests, so only one ( $D_0 = 1.54\text{mm}$ ) is displayed ( $\bar{k} \approx 0.56\text{mm}^2/\text{s}$ ). The droplet continues to vaporize after flame extinction, thus the continued droplet history after the flame data ends. The graph shows a sparse subset of the experimental data for clarity.

Figure 5 shows the effect of ignition energy on the burning history. The variation in ignition energy results from changing the time duration of the igniter ( $\tau_{ig}$ ). The two ignition times in Figure 5 are 0.7 and 1.2 s and  $D_0$  is 1.7mm for both tests. Time zero in this (and all graphs) corresponds to igniter withdraw. For the longer ignition time, a flame appears well before igniter withdraw. The results show that changes in the ignition energy do not noticeably affect  $k$ ,  $\bar{k}$  and minimally affect  $D_{ext}$  in these ambient conditions. The ignition energy, however, significantly influences flame size and standoff. Specifically, this increase in ignition time increases the flame diameter immediately after ignition by approximately 25 percent. This difference in flame size persists throughout the test with the flame size at extinction much larger for the longer ignition time (higher energy) case.

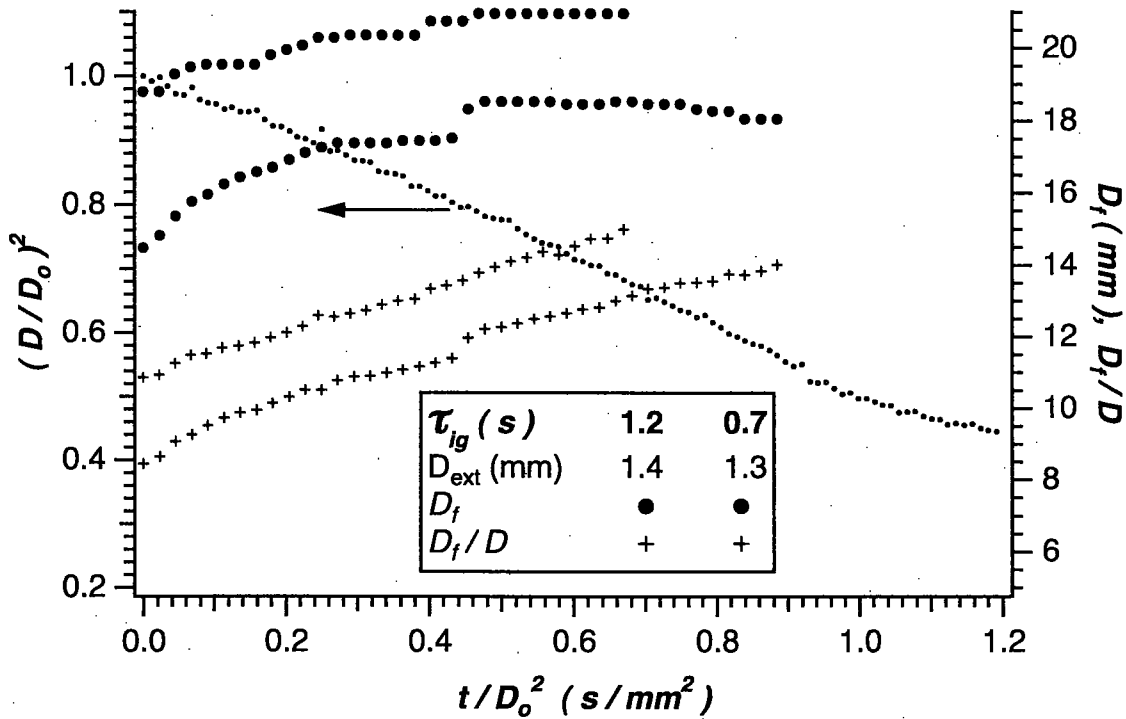


Figure 5. Combustion histories for two droplets ( $D_0 = 1.7\text{mm}$ ) with different ignition energies burning in  $X_{O_2} = 0.15$  and  $P = 90\text{mmHg}$  ambients. The droplet histories were nearly identical for all of the tests, so only one ( $\tau_{ig} = 0.7$ ) is displayed. The droplet continues to vaporize after flame extinction, thus the continued droplet history after the flame data ends. The graph shows a sparse subset of the experimental data for clarity.

### 3. Numerical Model

#### 3.1. Model Description

The numerical model is one-dimensional and transient in both the liquid and gas phase. The gas-phase model assumes one-step, second-order overall Arrhenius reaction, constant specific heats and thermal conductivity, constant Lewis number for each species (although different species can have different, constant Lewis numbers), ideal gas behavior, and no buoyant force[11]. The last assumption allows a simplified treatment of the momentum equation[12], which assumes potential flow and that the product ( $\rho T$ ) is a constant. The igniter is a source term in the energy equation at a particular region in the gas-phase. The model includes flame radiative losses from carbon dioxide and water vapor (gray gas treatment). The dimensional equations for the gas-phase are:

$$\frac{1}{r^2} \frac{\partial}{\partial r} \left( r^2 \frac{\partial \Phi}{\partial r} \right) = \frac{Q w_F - \dot{q}_r}{\rho_\infty C_p T_\infty} \quad (1)$$

$$\rho \frac{\partial Y_i}{\partial t} + \rho u_r \frac{\partial Y_i}{\partial r} - \frac{1}{r^2} \frac{\partial}{\partial r} \left( \rho D_i r^2 \frac{\partial Y_i}{\partial r} \right) = \nu_i w_F \quad (2)$$

$$\rho C_p \frac{\partial T}{\partial t} + \rho C_p u_r \frac{\partial T}{\partial r} - \frac{1}{r^2} \frac{\partial}{\partial r} (\lambda_g r^2 \frac{\partial T}{\partial r}) = Q w_F - \dot{q}_r + \dot{q}_l \quad (3)$$

$$w_F = \mathcal{A} \rho^2 Y_o Y_F \exp\left(-\frac{E}{\mathcal{R}T}\right) \quad (4)$$

The one-dimensional energy equation for the liquid phase is:

$$\frac{2}{r} \frac{\partial T}{\partial r} + \frac{\partial^2 T}{\partial r^2} = \frac{1}{\alpha_L} \frac{\partial T}{\partial t} \quad (5)$$

The gas-phase radiative loss is  $\dot{q}_r = A\sigma(T^4 - T_\infty^4)$ . The mean absorption coefficient,  $A$ , is  $A = 0.4(P_{CO_2} A_p^{CO_2} + P_{H_2O} A_p^{H_2O})$ [13]. The multiplication factor of 0.4 reflects the non-optically thin nature of the flame and the possible overestimate of the Planck-mean absorption data[14].

The boundary conditions at the gas/liquid interface are:

$$-\lambda_L \frac{\partial T}{\partial r}|_L + \lambda_g \frac{\partial T}{\partial r}|_g - \dot{q}_{rs} = \rho u_r \mathcal{L} \quad (6)$$

$$\rho \mathcal{D}_F \frac{\partial Y_F}{\partial r} = \rho u_r (1 - Y_F) \quad (7)$$

$$Y_F|_{surface} = \frac{P_v M_F}{P \bar{M}} \quad (8)$$

$$\rho \mathcal{D}_i \frac{\partial Y_i}{\partial r} = \rho u_r Y_i \quad (i = O_2, CO_2, H_2O) \quad (9)$$

Equations 6, 7 and 8 represent three equations for the three unknowns at the droplet surface,  $T$ ,  $Y_F$  and  $u_r$ . The radiative loss from liquid surface is  $\dot{q}_{rs} = \epsilon\sigma(T_S^4 - T_\infty^4)$  where  $\epsilon = 0.8$ . The far-field boundary conditions are ambient temperature and oxygen mole fraction, and no carbon dioxide, fuel or water vapor. The far-field boundary condition for the reduced momentum equation is  $u_r = 0$  and the boundary condition at the droplet surface comes from solving Eq. 6 for  $u_r$ .

The fuel is decane and its physical properties are in the nomenclature section. The activation energy,  $E$ , of the reaction is 30 kcal/mole. The pre-exponential factor,  $\mathcal{A}$ , has a value such that the flame extinguishes when the droplet is at an experimentally measured diameter ( $D_{ext}$ ), currently  $8 \times 10^{-4}$  cm.

### 3.2. Model Solution Procedure

The governing equations above become a tri-diagonal system of equations after discretization. The diffusion terms use a central difference operator while the convective terms use an upwind difference. There is an additional convective term to account for the fact that the grid moves with time. This is a result of non-dimensionalizing by  $R(t)$  [9]. The unsteady terms use a backward difference operator making the entire formulation implicit. The non-dimensional radial coordinate is  $\hat{r} = \tan \bar{r}$ , so the domain from the droplet surface to the ambient becomes  $\pi/4$  to  $\pi/2$ . There are 500 variably-spaced grid points in the  $r$ -direction. Near the droplet surface the smallest cell size is

( $0.01\bar{r}$ ), ( $0.1\bar{r}$ ) in the flame zone, and then expands with increasing distance from the droplet. The small grid size is necessary near the droplet surface to accurately determine the temperature gradient at the droplet surface (which in turn determines the burning rate constant and convective field).

The initial condition is a cold ambient profile with no fuel vapor. The igniter is a source term in the energy equation,  $q_I$ , 4-5 mm from the droplet surface, 1-2 mm in width with an energy generation rate between  $\approx 1 - 2 \text{ cal/cm}^3/\text{s}$ . These values closely approximate the energy supplied to the gas phase by the hot-wire in the experiments. The source term reduces linearly in magnitude (to zero) as the gas phase temperature in the ignition zone increases from 600 K to 1800 K. This decrease simulates the reduced heat transfer from the hot wire to the gas phase as the gas temperature increases. The results show that the best agreement between the model and experiment (post-ignition) occurs when the numerical model closely predicts the experimentally observed pre-ignition behavior (droplet size change, ignition delay time).

### 3.3. Model Results

Figure 6 shows a comparison of an experiment and a model prediction for a droplet burning in a  $P = 120 \text{ mm.Hg}$ ,  $X_{O_2} = 0.15$  oxygen mole fraction ambient. The  $D_{ext}$  are 0.76 and 0.69 mm for the experiment and model, respectively. The agreement between the model and experiment for the droplet burning history is excellent. The predicted flame diameter ( $D_f$ ) and it's temporal behavior are consistent with the experiment, except near the end of the test. Near extinction, the model predicts that the flame size and standoff ( $D_f/D$ ) will decrease until extinction and the experiment shows that the flame standoff increases continuously until extinction.

Figure 7 shows detailed radial profiles of gas temperature ( $T_g$ ), carbon dioxide mass fraction ( $Y_{CO_2}$ ), water vapor mass fraction ( $Y_{H_2O}$ ) and fuel vapor reaction rate ( $w_F$ ) for the model prediction in Figure 6. This Figure presents three times: immediately after ignition (A); midway through the burn (B); and close to extinction (C). The maximum gas temperature decays to approximately 1500 K within 0.1 s after ignition. The maximum gas temperature then remains relatively constant until just before flame extinction. This behavior is consistent with blowoff extinction where the flame extinguishes when the residence time is not sufficient for chemical reaction[15]. While the mechanism for extinction is blowoff (as opposed to radiant extinction), radiation loss from the flame zone is still important in these flames. The flame temperature and  $D_{ext}$  for an identical model prediction only neglecting radiant loss are approximately 1600 K and 0.30 mm, respectively. This emphasizes the potential importance of radiant loss even if it is not the dominant mechanism for flame extinction. The model does not include broad-band radiative loss (i.e. soot emission), but the flames in the experiments are dim and blue so radiative loss from soot is not significant.

Figure 8 shows the average burning rate constant,  $\bar{k}$ , as a function of ambient oxygen mole fraction. The initial droplet size was 1.8 mm and the ambient pressure

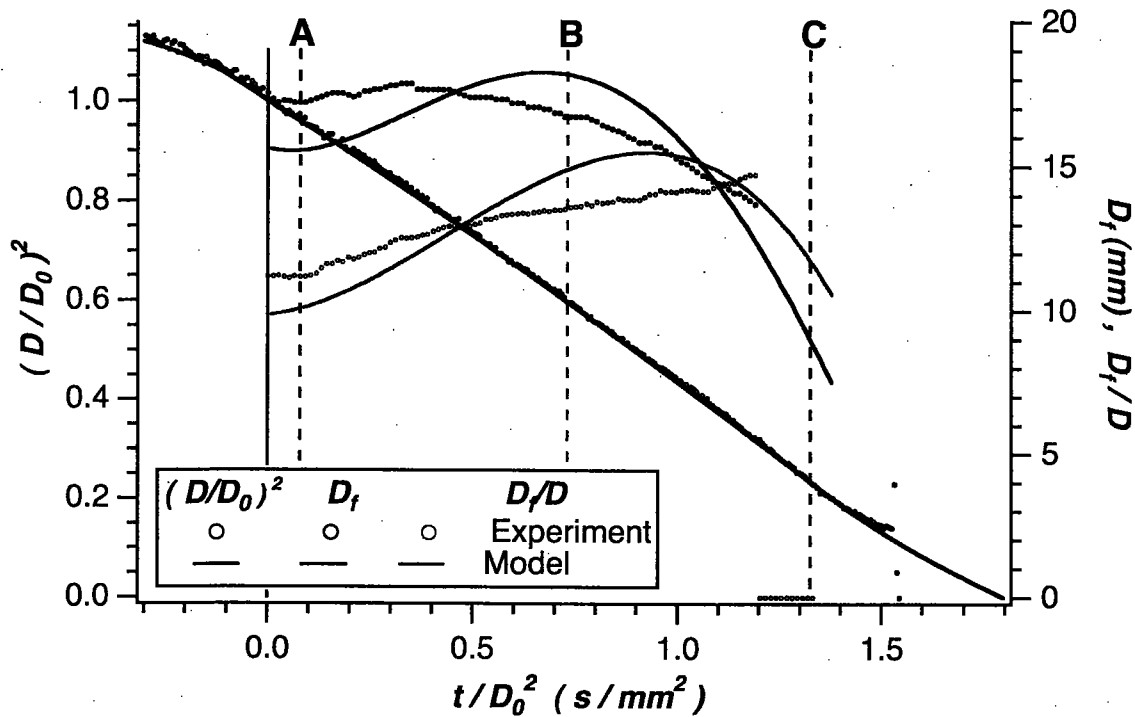


Figure 6. Numerical model results (compared to experiment) of a  $D_0 = 1.7\text{ mm}$  droplet in a  $X_{O_2} = 0.15$ ,  $P = 120\text{ mmHg}$  ambient. The flame in the experiment exists for slightly longer than in the graph, but was nearly invisible and difficult to measure (the SiC fiber indicates a flame was present).

was  $190\text{ mmHg}$  for all of the model results. Further, the ignition parameters (location and magnitude) were identical for all of the model runs. The initial droplet sizes in the experiments ranged from  $1.2$  to  $2.0\text{ mm}$ , and included results in different facilities (GRC 2.2 and 5.2 second drop towers and the 10 second Japan Microgravity Center), and in some cases different ignition energies. The range of experimental conditions explains some of the scatter in the experimental data.

Figure 9 shows comparisons between the model and experiments for average burning rate constant (9a) and extinction droplet diameter (9b) as a function of pressure. The  $X_{O_2}$  and  $D_0$  are  $0.15$  and  $1.8\text{ mm}$  respectively, for the numerical model data. The experimental initial droplet diameters ranged from  $1.5$  to  $2.0\text{ mm}$ , and there were variations in the facility and ignition conditions. The results for the average burning rate constant show reasonable agreement between the model and experiment considering the uncertainty in the experimental data and the simplifications in the numerical model.

The model predictions and experimental data for  $D_{ext}$ , however, do not agree quantitatively. While the model predicts the experimental  $D_{ext}$  at  $120\text{ mmHg}$ , we note that the pre-exponential factor ( $\mathcal{A}$ ) has a value to ensure agreement at this particular condition. Because of the influence of the support fiber, the  $D_{ext}$  is difficult (or impossible) to measure experimentally at pressures higher than  $120\text{ mmHg}$ . At

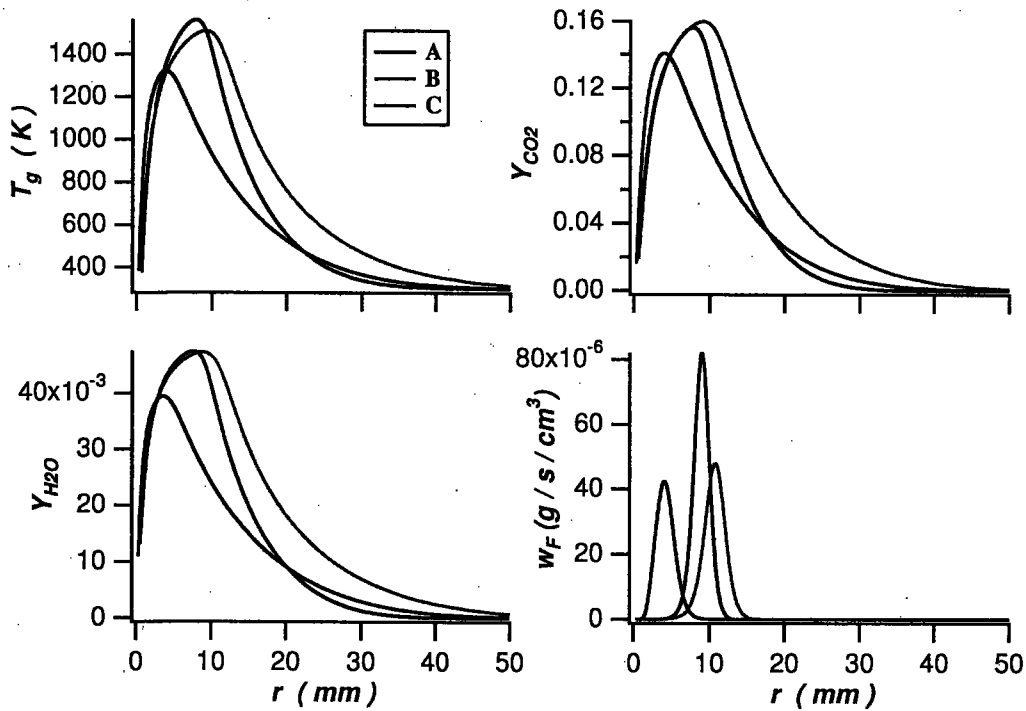


Figure 7. Detailed radial profiles of gas temperature ( $T_g$ ), carbon dioxide and water vapor mass fractions ( $Y_{CO_2}$  and  $Y_{H_2O}$ , respectively) and fuel vapor reaction rate ( $w_F$ ) for three times for the test in Figure 6.

ambient pressures less than  $120\text{mmHg}$ , the model predicts a much stronger dependence of extinction droplet diameter on pressure than that observed experimentally. In fact, at pressures below  $110\text{ mm Hg}$ , the model shows flame extinction almost immediately after ignition (or the model shows no ignition), where the experiments show a spherical flame burning for a short time followed by extinction. The discrepancy between the model and the experiment in the  $D_{ext}$  predictions is due to the simplified single-step chemistry in the model.

Figure 10 shows the predicted influence of ignition on the burning history for three tests where the ignition time varied from  $1.0$  to  $1.4\text{ s}$ . Because the droplet history for the three tests was nearly identical, the graph displays only one. The nearly identical droplet histories means that the burning rate constant is not significantly influenced by the ignition time ( $\bar{k} = 0.56, 0.58$  and  $0.58\text{ mm}^2/\text{s}$  for  $t_{ig} = 1.0, 1.2$  and  $1.4\text{ s}$ , respectively). Further, the extinction droplet diameters for the three tests are nearly identical ( $D_{ext} = 0.67, 0.66$  and  $0.66\text{ mm}$  for  $t_{ig} = 1.0, 1.2$  and  $1.4\text{ s}$ , respectively). This near independence of  $k$  (and  $\bar{k}$ ) and  $D_{ext}$  on ignition time is in reasonable agreement with the small changes in the experiments (Fig. 5). Figure 10 shows that the ignition time strongly influences the initial flame size. As the ignition time increases, the initial flame position moves further from the droplet. This agrees both qualitatively and quantitatively with the experimental results in Figure 5. Later in the droplet lifetime,

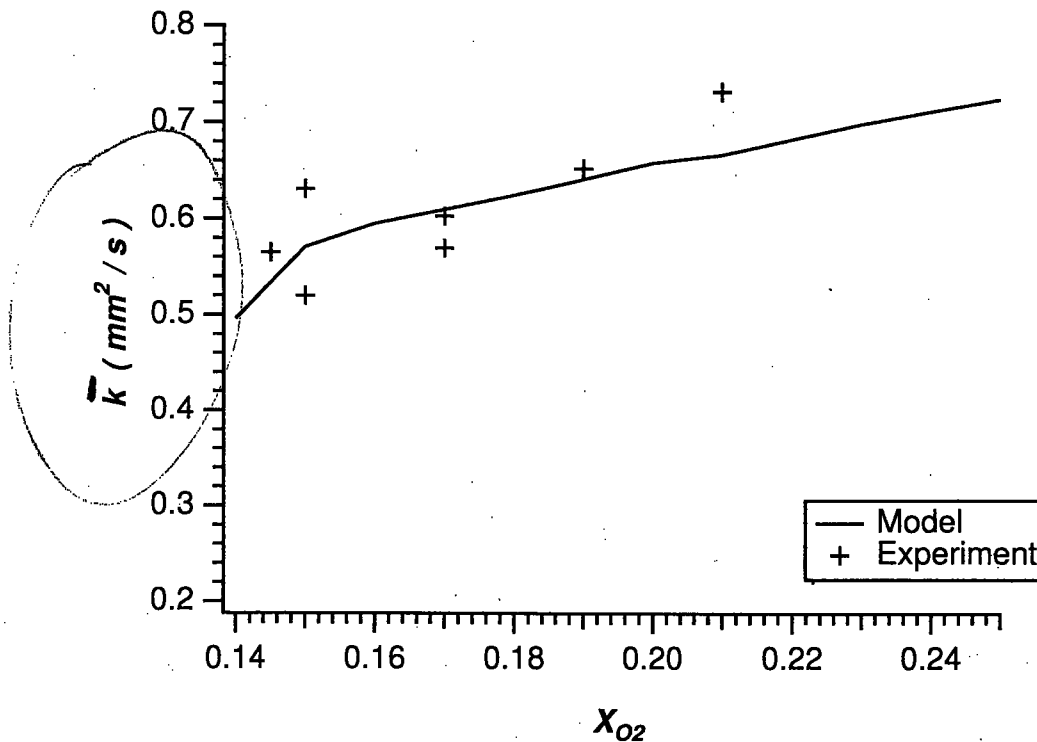


Figure 8. Comparison of experimental results and numerical model predictions for  $\bar{k}$  as a function of  $X_{O_2}$  for  $P = 120 \text{ mmHg}$ .

the model predicts that the flame histories merge and the flame seems to 'forget' the initial condition. The experiments show, however, that the ignition transients persist throughout the droplet lifetime. Part of the difference is due to the different pressures ( $90 \text{ mmHg}$  in the experiment versus  $120 \text{ mmHg}$  in the model) which means that the droplet lifetimes in the experiments were considerably shorter. The experimental flame histories for different ignition times may merge for ambient conditions with longer flame lifetimes.

#### 4. Discussion

The numerical model accurately predicts the temporal behavior of both the droplet and flame. This agreement requires suitable values for the average gas-phase thermo-physical and chemical kinetic properties. The fact that the droplet history agrees is not surprising, because even the simplest formulation (e.g. [1]) will produce accurate estimates of the burning rate constant, as long as reasonable properties are used in the formulation. Simplified models, however, do not predict accurate flame sizes. The current model provides reasonable agreement for flame size as a function of time.

One unexpected result of the modeling efforts was importance of matching the ignition source term in the model with the igniter characteristics in the experiments.

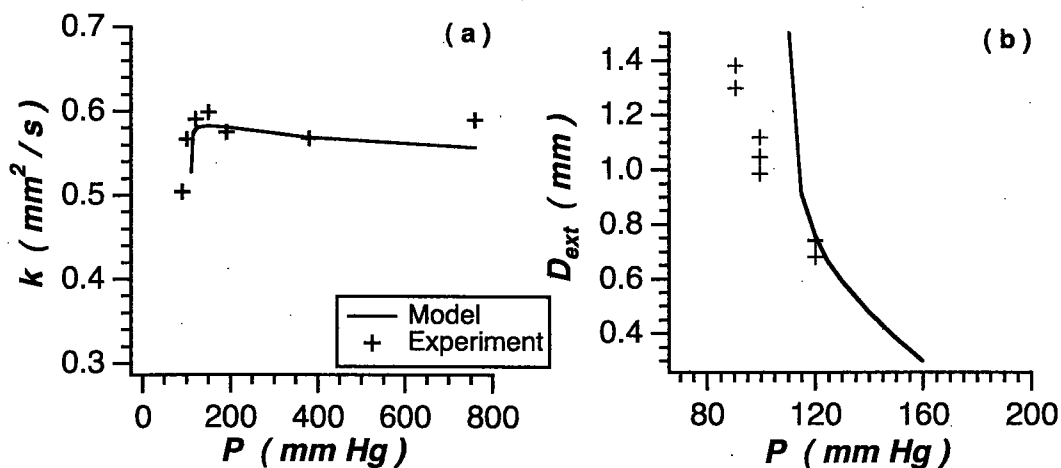


Figure 9. Comparison of experimental results and numerical model predictions for (a)  $\bar{k}$  and (b)  $D_{\text{ext}}$  as a function of  $P$  in  $X_{O_2} = 0.15$  ambients.

Specifically, early in the model development, there was a large discrepancy between the model and experiment. The model either predicted that the droplet burned to completion or extinguished quickly after ignition depending on the value of  $\mathcal{A}$ . This inability to predict extinction disappeared and the model predictions improved when the igniter location and energy more closely matched the experiment and the model accurately predicted the pre-ignition vaporization behavior.

One reason for this sensitivity is the degree of pre-ignition heating of the liquid phase, particularly for the relatively large droplets in the present study. With the ignition region closer to the droplet surface, the droplet ignites quickly but at a relatively cold temperature. The rate of heat loss to the cold droplet during combustion then significantly affects the extinction behavior of the flame. The heat loss to the droplet is directly proportional to the thermal conductivity of the liquid fuel. The current model assumes that the energy transport in the liquid is purely diffusional. A number of studies (e.g. [19, 20]) exist, however, showing that significant convective flows, driven by surface tension gradients, exist inside these relatively large liquid droplets. These surface tension gradients can be either thermally or solutally driven, although the later is unlikely in the present study. It may be possible to use a modified thermal conductivity[21] to more closely approximate the actual thermal transport inside the droplet. We note, however, that the presence of the support fiber in the experiments has an unknown influence on

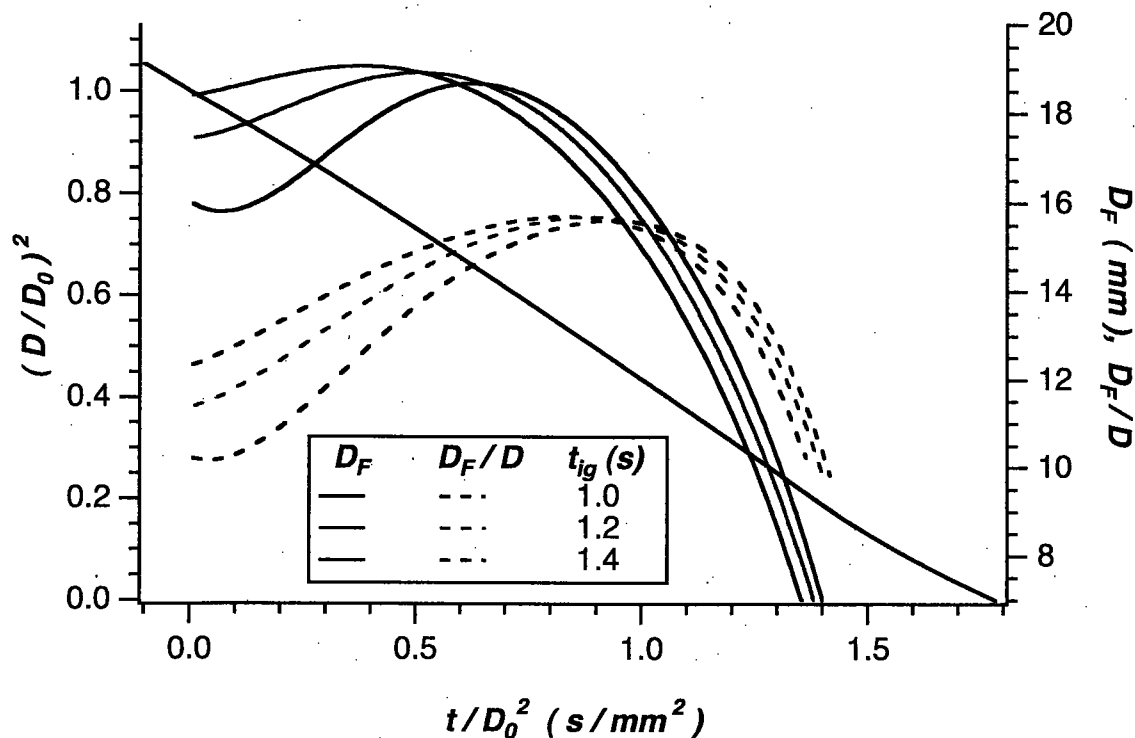


Figure 10. Numerical model results for the burning history of a  $D_0 = 1.5\text{mm}$  droplet burning in a  $P = 120\text{mm.Hg}$ ,  $X_{O_2} = 0.15$  ambient with three different ignition energies. The variation in ignition energy results, similar to the experiments, from changes in the ignition time.

any convective flows inside the droplet.

The sensitivity to ignition may occur because combustion takes place in ambients that are close to the flammability limit. The current model predicts a limiting  $Y_{O_2}$  of approximately 0.14 that can support combustion for the droplet size and pressure range in this study. The limit predicted by the model is nearly identical to the experimental limit observed by Easton[22].

The transient behavior of the flame standoff in the present experiments suggests the potential importance of fuel vapor accumulation [24, 25] between the droplet and the flame. When the fuel vaporization rate is greater than the total fuel consumption rate at the flame, fuel can accumulate between the droplet and the flame. Law and co-workers [24] showed that this phenomena can explain the experimentally observed growth in the flame standoff ratio with time (especially early in the droplet lifetime). The ratio ( $\delta$ ) of the fuel vapor consumption rate to the fuel vaporization rate is easy to evaluate in the present model.

$$\delta = \frac{2 D^2}{\rho_L k} \int_1^\infty \bar{r}^2 w_F d\bar{r} \quad (10)$$

The  $w_F$  in Eq. 12 is the radial variation of the fuel vapor consumption rate such as that in Fig. 7.

He's [25] analysis indicates that the motion of the flame front is important and the fuel vapor consumption rate at the flame can differ from the fuel vaporization rate for the ambient conditions in the present study. In this case, their model predicts a flame size that increases initially with time, reaches a maximum and then decreases in response to the shrinking droplet. The model further predicts that the flame standoff ratio will increase continuously with time. This is in qualitative agreement with the flame behavior in the present experiments. Their

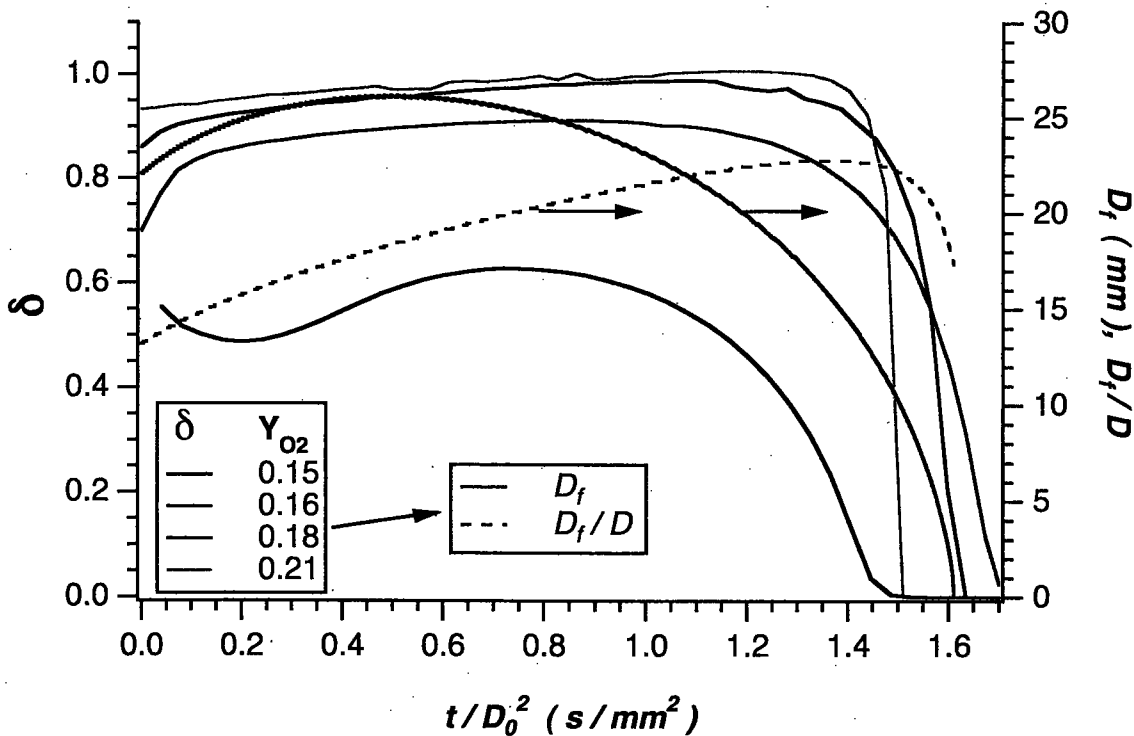


Figure 11. Fuel vapor consumption to fuel vaporization rate ratio ( $\delta$ ) as a function of non-dimensional time for different  $X_{O_2}$  ambients ( $P = 190\text{mm.Hg}$ ). The flame data are for the  $X_{O_2} = 0.18$  ambient.

Figure 11 shows the model prediction of the temporal variation in  $\delta$  with time for different  $X_{O_2}$  ambients ( $P = 190\text{mm.Hg}$ ). For  $X_{O_2}$  greater than 0.16,  $\delta$  is greater than 0.9 for nearly all of the droplet lifetime, and gradually increases throughout the burn approaching nearly 1.0 before decreasing abruptly near fuel droplet burnout. Figure 11 also shows the temporal variation of  $D_f$  and  $D_f/D$  for the  $Y_{O_2} = 0.18$  case. The results clearly show that  $\delta$  is close to 1.0 even though  $D_f/D$  increases continuously until very close to droplet burnout.

Figure 11 further shows that when  $X_{O_2} = 0.16$ ,  $\delta$  increases quickly to 0.8, then gradually increases to 0.9 before decreasing (more gradually than the higher  $X_{O_2}$  cases) near fuel droplet burnout. The temporal behavior of  $\delta$  is very different in the  $X_{O_2} = 0.15$  ambient, with the  $\delta$  less than 0.6 for almost the entire droplet lifetime. A detailed

examination of the  $w_F$  profiles, however, shows this decrease is, at least in part, due to fuel leakage through the flame front.

## 5. Conclusions

This paper presents experiments involving the combustion of single decane droplets in microgravity. The experiments are over a range of ambient pressures and oxygen mole fractions, initial droplet sizes and ignition energies. The data are useful for the validation of detailed numerical models of droplet combustion which in turn can form the basis of sub-models for spray combustion models. The data regarding extinction droplet sizes enable the evaluation and validation of kinetic mechanisms in a simplified, computationally tractable geometry.

The numerical model accurately predicts the burning behavior of the droplet, both the droplet and flame history. This good agreement requires accurate modeling of the ignition which in turn requires accurate modeling of the pre-ignition vaporization behavior. Both the experiments and model show transient flame behavior which suggests the importance of fuel vapor accumulation between the droplet and flame. The model results show, however, that the ratio of the mass rate of fuel consumption (at the flame) to fuel vaporization is nearly 1.0 suggesting that fuel vapor accumulation alone cannot explain the observed transient flame behavior.

HOW ABOUT GAS  
PHASE RAD IN  
PREDICTING Ext ?

## Acknowledgments

The authors would like to thank J.S. T'ien, Y. Shu and P. Chang for the source code of the candle flame (the basis of the current model) and their input on the current model. PMS and DLD would like to thank I. Goodman and D. Lenhart for their assistance with the NASA GRC experiments and analysis of the experimental data. The authors would like to thank S. Honma, K. Ikeda, K. Kitano, and H. Nagaiishi for their assistance with the JAMIC experiments. DLD thanks K.A. Kutler for her critical review of the manuscript.

## Nomenclature

$A$	mean absorption coefficient
$A_P^i$	Planck mean absorption coefficient for species $i$
$A$	Pre-exponential factor ( $8 \times 10^{14} \text{ cm}^3/\text{g/s}$ )
$C_p$	gas-phase specific heat ( $0.362 \text{ cal/g/K}$ )
$D_i$	binary diffusion coefficient of species $i$
$D$	droplet diameter
$D_0$	initial droplet diameter
$D_f$	flame diameter
$Da$	Damköhler number

$E$	activation energy ( $3 \times 10^4$ cal/mole)
$k$	instantaneous burning rate constant
$\bar{k}$	average burning rate constant
$\mathcal{L}$	latent enthalpy of vaporization (varies with T, $\approx 70$ cal/g at $T_b$ )
$Le_i$	Lewis number of species $i$ (2, 1.1, 1.4 and 0.83 for F, O <sub>2</sub> , CO <sub>2</sub> and H <sub>2</sub> O, respectively)
$M_i$	molar mass of species $i$
$\bar{M}$	average molar mass
$P_i$	partial pressure of species $i$
$P_v$	equilibrium fuel vapor pressure at surface temperature
$Q$	heat release per unit mass of fuel (11472 cal/g)
$q_r$	gas phase radiative energy loss (cal/s/cm <sup>3</sup> )
$q_{rs}$	surface radiative energy loss (cal/s/cm <sup>2</sup> )
$q_I$	ignition energy (cal/s/cm <sup>3</sup> )
$r$	radial coordinate
$\bar{r}$	non-dimensional radial coordinate $\bar{r} = \frac{r}{R}$
$\hat{r}$	transformed radial coordinate $\hat{r} = \tan \bar{r}$
$t$	time
$R$	radius of the droplet
$\mathcal{R}$	universal gas constant
$T$	temperature
$T_b$	boiling temperature of the fuel
$u$	gas velocity
$w_F$	fuel vapor reaction rate per unit volume (g/s/cm <sup>3</sup> )
$X$	mole fraction
$Y$	mass fraction
$\alpha$	gas-phase thermal diffusivity
$\alpha_L$	liquid-phase thermal diffusivity
$\lambda$	gas-phase thermal conductivity ( $1.05 \times 10^{-4}$ cal/K/s/cm)
$\lambda_L$	liquid-phase thermal conductivity ( $2.82 \times 10^{-4}$ cal/K/s/cm)
$\Phi$	$\phi - \frac{\lambda}{\rho_\infty C_p} \frac{T}{T_\infty}$
$\phi$	velocity potential, $u_r = \frac{\partial \phi}{\partial r}$
$\rho$	gas density
$\rho_L$	liquid fuel density
$\nu_i$	stoichiometric coefficient for species $i$

## References

- [1] Godsave G A E 1953 *Proc. Comb. Inst.* 4 818
- [2] Kumagai S and Isoda H 1956 *Proc. Comb. Inst.* 6 726
- [3] Williams F A 1985, *Combustion Theory*, Second Edition (New York: Addison-Wesley)
- [4] Choi M Y and Dryer F L 2001 *Microgravity Combustion, Fire in Free Fall* (New York: Academic Press) 183

- [5] Card J M and Williams F A 1992 *Combust. Flame* **91** 187
- [6] Cho S Y, Yetter R A and Dryer F L *J. Comput. Phys.* **102** 160
- [7] Struk P M, Dietrich D L, Ikegami M and Xu G 2002 *Proc. Comb. Inst.* **29** 609.
- [8] Struk P M, Ackerman M, Nayagam V and Dietrich D L 1998 *Microgravity Sci. Tech.* **XI/4** 144
- [9] Law C K and Sirignano W A 1977 *Combust. Flame* **28** 175
- [10] Law C K, Chung S H and Srinivasan N 1980 *Combust. Flame* **38** 173
- [11] Dietrich D L, Ross H D, Shu Y, Chang P and Tien J S *Combust. Sci. Tech.* **156** 1
- [12] Baum H R 1990 *Modeling in Combustion Science*, ed. Buckmaster J and Takeno T (New York: Springer) 118
- [13] Abu-Romia M M and Tien C L 1967 *ASME J. Heat Transfer* **89C** 321
- [14] Liu K V, Lloyd J R and Yang K T 1981 *Int. J. Heat Mass Transfer* **24**(12) 1959
- [15] Law C K 1975 *Combust. Flame* **24** 89
- [16] Chao B H, Law C K and Tien J S 1990 *Proc. Comb. Inst.* **23** 523
- [17] Nayagam V, Haggard J B, Colantonio R, Marchese A J, Dryer F L, Zhang B L and Williams F A 1998 *AIAA J.* **26** 1369
- [18] Marchese A J and Dryer F L 1997 *Combust. Flame* **105** 104
- [19] Dietrich D L, Haggard J B, Dryer F L, Nayagam V, Shaw B D and Williams F A 1996 *Proc. Comb. Inst.* **26** 1201
- [20] Shaw B D and Chen A G 1997 *Microgravity Sci. Tech.* **X/3** 136
- [21] Talley D G and Yao S C 1986 *Proc. Comb. Inst.* **21** 609
- [22] Easton J W 1998 *Large Diameter, Radiative Extinction Experiments with Decane Droplets in Microgravity* Masters Thesis, Case Western Reserve University
- [23] Marchese A J, Dryer F L and Nayagam V 1999 *Combust. Flame* **116** 432
- [24] Law C K, Chung S H and Srinivasan N 1980 *Combust. Flame* **38** 173
- [25] He L, Tse S D and Law C K 1998 *Proc. Comb. Inst.* **27** 1943